which are unstable in many reactions (*42–45*), also underwent this process to form the corresponding product from trans-hydroheteroarylation of diphenylacetylene. Reaction of a heteroaryl boronic acid with an internal alkyne possessing alkyl substituents also formed the product of hydroheteroarylation.

Selected examples of the second type of alkyne hydroarylation that we discovered involving aryl halides and triethylsilane are shown in Fig. 7. Although further studies are needed to identify the most effective combination of catalyst and reducing agent, our current studies show that the reactions of aryl halides containing potentially reactive functional groups, as well as heteroaryl halides, form the trisubstituted alkenes with good-to-moderate selectivity for the product from formal trans-addition.

This approach to reaction discovery holds considerable potential for purposes beyond those revealed in the current work. For example, this system could be used to explore reactions with additives, such as oxidants, reductants, acids, and bases, and to explore reactions of two substrates with a third component, such as carbon monoxide or carbon dioxide. It could also be used to examine the reactivity of a single class of ligand with various organic substrates and transition metal–catalyst precursors. Thus, we anticipate that this approach to reaction discovery will provide a general and adaptable platform suitable for use by a wide range of laboratories for the discovery of a variety of catalytic reactions.

References and Notes

1. H. S. Eleuterio, *J. Mol. Catal.* **65**, 55 (1991).
2. K. Fischer, K. Jonas, P. Misbach, R. Stabba, G. Wilke, *Angew. Chem. Int. Ed. Engl.* **12**, 943 (1973).
3. J. P. Stambuli, J. F. Hartwig, *Curr. Opin. Chem. Biol.* **7**, 420 (2003).
4. J. Wieland, B. Breit, *Nat. Chem.* **2**, 832 (2010).
5. P. J. Fagan, E. Hauptman, R. Shapiro, A. Casalnuovo, *J. Am. Chem. Soc.* **122**, 5043 (2000).
6. T. R. Boussie et al., *J. Am. Chem. Soc.* **125**, 4306 (2003).
7. A. B. Beeler, S. Su, C. A. Singleton, J. A. Porco Jr., *J. Am. Chem. Soc.* **129**, 1413 (2007).
8. H. Kinoshita, O. J. Ingham, W. W. Ong, A. B. Beeler, J. A. Porco Jr., *J. Am. Chem. Soc.* **132**, 6412 (2010).
9. M. W. Kanan, M. M. Rozenman, K. Sakurai, T. M. Snyder, D. R. Liu, *Nature* **431**, 545 (2004).
10. M. M. Rozenman, M. W. Kanan, D. R. Liu, *J. Am. Chem. Soc.* **129**, 14933 (2007).
11. C. Markert, P. Rösel, A. Pfaltz, *J. Am. Chem. Soc.* **130**, 3234 (2008).
12. C. A. Müller, A. Pfaltz, *Angew. Chem. Int. Ed.* **47**, 3363 (2008).
13. A. Teichert, A. Pfaltz, *Angew. Chem. Int. Ed.* **47**, 3360 (2008).
14. J. W. Szewczyk, R. L. Zuckerman, R. G. Bergman, J. A. Ellman, *Angew. Chem. Int. Ed.* **40**, 216 (2001).
15. P. Chen, *Angew. Chem. Int. Ed.* **42**, 2832 (2003).
16. C. Hinderling, P. Chen, *Int. J. Mass Spectrom.* **195-196**, 377 (2000).
17. H. M. Geysen et al., *Chem. Biol.* **3**, 679 (1996).
18. G. T. Copeland, S. J. Miller, *J. Am. Chem. Soc.* **123**, 6496 (2001).
19. B. M. Cole et al., *Angew. Chem. Int. Ed. Engl.* **35**, 1668 (1996).
20. K. D. Shimizu et al., *Angew. Chem. Int. Ed. Engl.* **36**, 1704 (1997).
21. M. B. Francis, E. N. Jacobsen, *Angew. Chem. Int. Ed.* **38**, 937 (1999).
22. All but one of these compounds are commercially available.
23. Previously, custom mass spectrometers have been used to analyze, by tandem MS-MS methods, the activity of charged catalysts for reactions conducted in the gas phase. These examples have focused on comparing several catalysts for a single reaction, such as olefin polymerization and olefin metathesis (*15*, *16*). Mass spectrometry has also been used to analyze the binding of encoded organic ligands to biological targets (*17*). Our approach does not require such encoding.
24. We used several additional design elements, including the placement of different substituents on aryl groups to discriminate between them by their distinct mass spectral fragmentation patterns.
25. Y. Nakao, S. Oda, T. Hiyama, *J. Am. Chem. Soc.* **126**, 13904 (2004).
26. P. Y. S. Lam et al., *Tetrahedron Lett.* **39**, 2941 (1998).
27. M. H. S. A. Hamid et al., *J. Am. Chem. Soc.* **131**, 1766 (2009).
28. Intermolecular hydroamination of an alkyne has been reported with complexes of Group IV metals that are air-sensitive and generally suffer from poor functional-group compatibility, and it has been catalyzed by complexes of the precious metals palladium, rhodium, and gold.
29. Classical additions of amines to alkynes are conducted with toxic mercury compounds.
29. L. Zhou, H.-F. Jiang, C.-J. Li, *Adv. Synth. Catal.* **350**, 2226 (2008).
30. J. Han, B. Xu, G. B. Hammond, *J. Am. Chem. Soc.* **132**, 916 (2010).
31. T. E. Müller, K. C. Hultzsch, M. Yus, F. Foubelo, M. Tada, *Chem. Rev.* **108**, 3795 (2008).
32. Reactions catalyzed by Cu(OAc)$_2$ yielded substantial product from Glaser coupling of the alkynes from a diyne.
33. Examples are limited to those catalyzed by an air-sensitive titanium complex and a single example catalyzed by a zinc complex.
34. E. Haak, I. Bytschkov, S. Doye, *Angew. Chem. Int. Ed.* **38**, 3389 (1999).
35. K. Alex, A. Tillack, N. Schwarz, M. Beller, *ChemSusChem* **1**, 333 (2008).
36. T. Hayashi, K. Inoue, N. Taniguchi, M. Ogasawara, *J. Am. Chem. Soc.* **123**, 9918 (2001).
37. X. Xu et al., *Tetrahedron* **66**, 2433 (2010).
38. P.-S. Lin, M. Jeganmohan, C.-H. Cheng, *Chemistry* **14**, 11296 (2008).
39. E.-i. Negishi et al., *Acc. Chem. Res.* **41**, 1474 (2008).
40. E.-i. Negishi, G. Wang, H. Rao, Z. Xu, *J. Org. Chem.* **75**, 3151 (2010).
41. Aryl boronic acids containing electron-donating substituents at the 4-position give ~1:1 mixtures of stereoisomers.
42. G. A. Molander, B. Canturk, L. E. Kennedy, *J. Org. Chem.* **74**, 973 (2009).
43. D. M. Knapp, E. P. Gillis, M. D. Burke, *J. Am. Chem. Soc.* **131**, 6961 (2009).
44. T. Kinzel, Y. Zhang, S. L. Buchwald, *J. Am. Chem. Soc.* **132**, 14073 (2010).
45. K. Billingsley, S. L. Buchwald, *J. Am. Chem. Soc.* **129**, 3358 (2007).

Ice Flow of the Antarctic Ice Sheet

E. Rignot,[1,2]* J. Mouginot,[1] B. Scheuchl[1]

We present a reference, comprehensive, high-resolution, digital mosaic of ice motion in Antarctica assembled from multiple satellite interferometric synthetic-aperture radar data acquired during the International Polar Year 2007 to 2009. The data reveal widespread, patterned, enhanced flow with tributary glaciers reaching hundreds to thousands of kilometers inland over the entire continent. This view of ice sheet motion emphasizes the importance of basal-slip–dominated tributary flow over deformation-dominated ice sheet flow, redefines our understanding of ice sheet dynamics, and has far-reaching implications for the reconstruction and prediction of ice sheet evolution.

Ice velocity is a fundamental characteristic of glaciers and ice sheets that measures the rate at which ice is transported from the interior regions toward the ocean, the location of preferred channels of ice transport, and how ice mass evolves with time. Traditional measurements from ground-based stations are limited relative to the size of the continent, leading to an incomplete picture of Antarctica. Satellite radar interferometry, or InSAR, has been successfully used to map glacier flow independent of cloud cover, solar illumination, or the presence of surface features (*1*). Until now, however, the vast extent of East Antarctica, which comprises 77% of the continent, has been devoid of quality data; only a few floating ice shelves have been mapped, and comprehensive velocity mapping has been limited to the lower reaches of key outlet glaciers (*2*).

Balance velocity calculated from ice thickness, surface slope, and snow accumulation data provides insights about the potential flow pattern of the ice sheet (*3*), but the technique assumes an ice sheet in mass equilibrium, which is not correct everywhere, and that ice flows perpendicular to surface contours, which is a

[1]Department of Earth System Science, University of California Irvine, Irvine, CA 92697, USA. [2]Jet Propulsion Laboratory, California Institute of Technology, Pasadena, CA 91109, USA.

*To whom correspondence should be addressed. E-mail: erignot@uci.edu

simplification of the gravitational driving stress equation of motion (4). The precision of balance velocity is affected by uncertainties in snow accumulation, major gaps in ice thickness data, and poor topographic coverage near the South Pole. Nor does the technique apply to floating ice shelves or replicate the correct width and extent of ice streams and tributaries (5). As a result, there is no clear picture of ice sheet motion at the continental scale, from topographic divides to a set of narrow, fast-moving glaciers that control most of the ice sheet discharge into the ocean. This lack of broad-scale detailed observation of ice motion has placed a fundamental limit on the capability and reliability of numerical models of ice sheet evolution (6).

On the eve of the international polar year, international space agencies worked together to enable a complete InSAR survey of Antarctica. We used spring 2009 data from RADARSAT-2 [Canadian Space Agency (CSA) and MacDonald, Dettwiler, and Associates Limited (MDA)]; spring 2007, 2008, and 2009 data from Envisat ASAR [European Space Agency (ESA)]; and fall 2007 to 2008 data from the Advanced Land Observing Satellite (ALOS) PALSAR [Japan Aerospace Exploration Agency (JAXA)], complemented by patches of CSA's RADARSAT-1 data from fall 2000 (7) and ESA's Earth Remote-Sensing Satellites 1 and 2 (ERS-1/2) data from spring 1996 (2). Each radar instrument contributes its unique coverage and performance level (fig. S1).

The final mosaic assembles 900 satellite tracks and more than 3000 orbits of radar data (Fig. 1). The data are georeferenced with a precision better than one pixel, here 300 m, to an Earth-fixed grid by using a digital elevation model (DEM) (8). Absolute calibration of the surface velocity data relies on control points of zero motion distributed along the coast (stagnant areas near ice domes or emergent mountains) and along major ice divides (areas of zero surface slope in the DEM) in a set of coast-to-coast advanced synthetic aperture radar (ASAR) tracks (fig. S1). The mapping precision varies with instrument, location, technique of analysis, repeat cycle, time period, and data stacking. Nominal errors range from 1 m/year along major ice divides with high data stacking to about 17 m/year in areas affected by ionospheric perturbations (fig. S2). In terms of strain rate, or changes in velocity per unit length, data noise is at the 3×10^{-4} per year level, which is sufficient to reveal effective strain rates along tributary shear margins over the vast majority of the continent (Fig. 2A).

Ice velocity ranges from a few cm/year near divides to a few km/year on fast-moving glaciers and floating ice shelves, or 5 orders of magnitude. The histogram in surface velocity has a bimodal distribution with a main peak at 4 to 5 m/year, corresponding to slow motion in East Antarctica, and a second peak at 250 m/year, driven by the fast flow of glaciers and ice shelves. The fastest glaciers, Pine Island and Thwaites, are several times faster than any other glacier

and unique in terms of how far inland fast flow prevails. This is indeed the sector of most rapid change at present, over the widest area, and with the greatest impact on total ice sheet mass balance (2). Other fastest-moving glaciers include the Larsen B glaciers in the peninsula, which accelerated in response to ice shelf collapse (9); the Ferrigno and Land glaciers in the west; and the Ninnis, Frost, Totten, Denman, and Shirase glaciers in the east.

There is reasonably good agreement between observed surface velocity and balance velocity (Fig. 2B) near ice divides; however, large differences exist within each basin and especially near the coast, demonstrating that the direct measurement of ice velocity is crucial to capture continental-wide ice motion accurately. Figure 1 reveals a wealth of new information. For instance, the exact pathway of ice along the coastline is not without surprise. In Queen Maud Land, the main trunk of Jutulstraumen is not to the south through Penck trough but to the east of Neumayer Cliffs (10). The Sør Rondane Mountains were known to deflect ice flow to the east and to the west

through Hansenbreen and Brydbreen glaciers, but the main ice sheet discharge is from two large (80-km) unnamed ice streams (named SøR Rondane and Belgica in Fig. 1 for convenience) that flow at 100 to 200 m/year around the Belgica Mountains for more than 500 km inland (11). Farther east, the fast-flowing core of Shirase Glacier does not extend far inland, but little-studied Rayner Glacier to the east flows above 100 m/year for more than 200 km inland, presumably along a deep subglacial trough (12). In the Antarctic Peninsula, the tributaries of Wilkins Ice Shelf and of the northern sector of George VI Ice Shelf abruptly transition to zero velocity when they mix with the floating ice shelves. We attribute this spectacular termination of the glaciers to massive rates of basal ablation of the ice shelves by the underlying warm ocean (13).

An interesting aspect is the spatial pattern of tributary flow. Each major glacier is the merger of several tributaries that extend hundreds of km inland. Although this was observed in the partial mapping of Siple Coast (14) and Pine Island (15), this is now observed over the entire ice sheet.
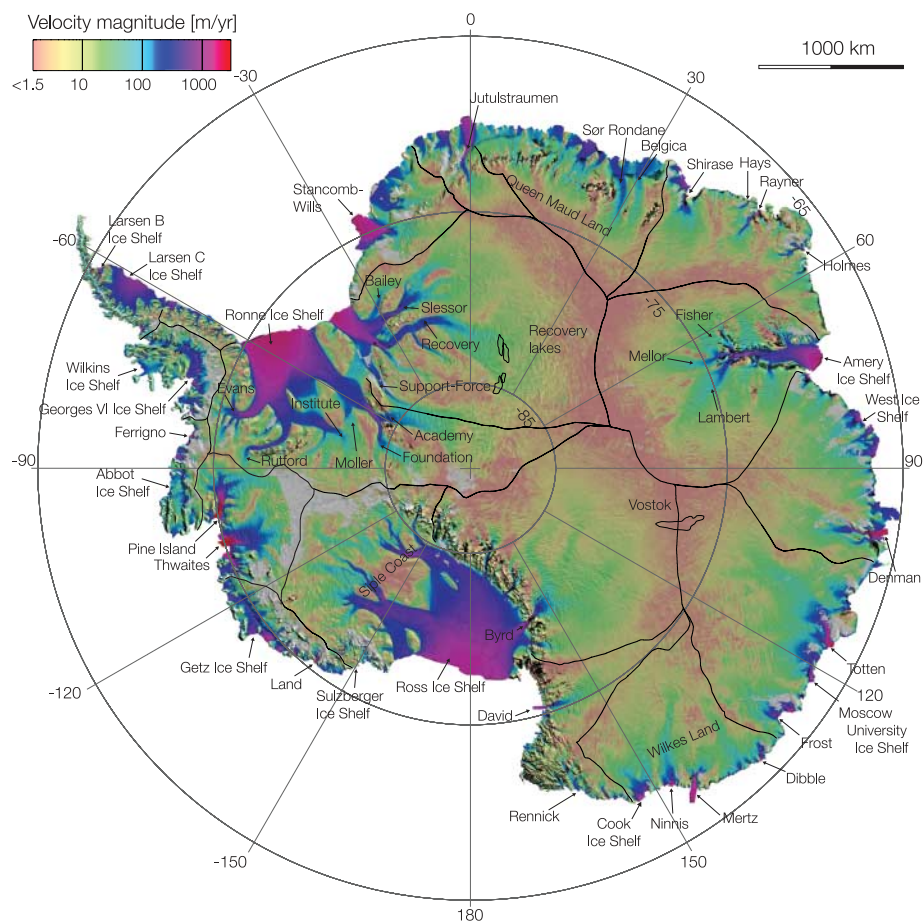
Fig. 1. Antarctic ice velocity derived from ALOS PALSAR, Envisat ASAR, RADARSAT-2, and ERS-1/2 satellite radar interferometry, color-coded on a logarithmic scale, and overlaid on a MODIS mosaic of Antarctica (22), with geographic names discussed in the text. Pixel spacing is 300 m. Projection is polar stereographic at 71°S secant plane. Thick black lines delineate major ice divides (2). Thin black lines outline subglacial lakes discussed in the text. Thick black lines along the coast are interferometrically derived ice sheet grounding lines (23).
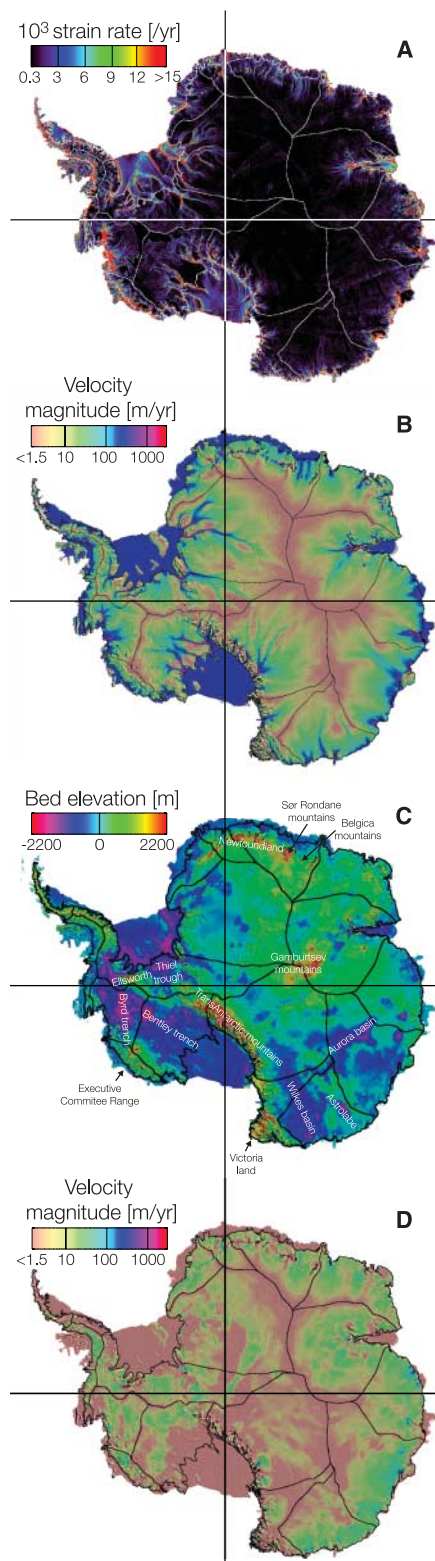
Fig. 2. (A) Effective strain rate, $\dot{\varepsilon}$, color-coded from 3×10^{-4} year^{-1} to greater than 15×10^{-3} year^{-1}; (B) balance velocity (3) color-coded on a logarithmic scale as in Fig. 1; (C) bed elevation (24) with geographic names discussed in the text; (D) surface velocity calculated from internal deformation with a creep parameter, $A = 9 \times 10^{-25}$ s^{-1} Pa^{-3}. Thick black lines in (B) to (D) and white lines in (A) delineate major ice divides (2) and grounding lines (23).

The map reveals to its full extent the dendritic nature of drainage systems, the anastomosing distribution of tributaries, the narrowing (acceleration) and widening (deceleration) of tributaries inland, and their extension well beyond grounding lines toward topographic divides. On Pine Island, Thwaites, and Siple Coast, the tributaries extend to ice divides everywhere that we have data. Pine Island and Rutford share a common source in the south that connects two different sides of West Antarctica. Furthermore, the velocity divide is offset to the east of the topographic divide by 10 to 15 km, which suggests uncertainties in DEM-derived ice divide or recent changes in ice dynamics and enhanced flow to the west. The western tributary of Foundation Ice Stream offers a natural division between East and West Antarctica flow that was not known before. Academy Glacier, a major eastern tributary of Foundation, extends to the west over the South Pole and to the east in parallel to Support-Force Ice Stream for more than 400 km, which is counter to the traditional view of well-defined drainage basins.

Our map reveals to their full extent the tributaries of Recovery, Slessor, and Bailey ice streams, which are grounded below sea level and are likely underlaid by thick marine sediments that favor rapid basal motion (16, 17). The tributaries share common sources that extend 1000 km inland of the grounding line through a meander of slow moving areas. Recovery Ice Stream's two main tributaries broaden inland and reach beyond the four subglacial lakes thought to be a possible source of fast motion (18). The presence of two subglacial lakes may accelerate the flow of the tributaries coming from the east, but this acceleration is nonexistent for the tributaries coming from the west. Similarly, at Lake Vostok, the largest subglacial lake in Antarctica, flow disturbances remain at the submeter scale per year (19) and are not expressed beyond the lake. The impact of the abrupt reduction in basal friction associated with subglacial lakes is not apparent anywhere in the broad pattern of ice sheet motion.

Bedrock topography has a clear impact on the flow pattern of ice (Fig. 2C). Restricted ice motion is observed over major subglacial (Gamburtsev) and around emergent mountains (Newfoundland, Sør Rondane, Victoria Land, TransAntarctic, Executive Committee Range, Ellsworth, and Graham Land), which deflect flow around them or limit flow through narrow glaciers. The tributaries of Lambert Glacier extend inland among slow-moving areas of higher ground, hence higher basal friction, with some tributaries emerging as narrow, fast streams at the flanks of the Gamburtsev Mountains, which is unexpected this far inland from the coast. The ice flowing down Byrd Glacier, the most extensive basin drained by a single glacier, originates from four tributaries that spread inland over more than 1000 km. The tributaries are wider and more diffuse than in the balance velocity map, which reveals a form of ice motion that is neither ice stream flow nor

ice sheet flow but an intermediate regime that we denote "patterned enhanced flow."

Conversely, major flow pathways do not follow the deepest subglacial basins; hence, the divide between Pine Island, Rutford, and Evans runs across Byrd and Bentley trenches, and the divide between Cook Ice Shelf and David Glacier runs across the Wilkes subglacial basin. Totten Glacier extends 1000 km inland through two major tributaries that reach the Aurora subglacial basin, alongside Denman, another marine-based fast-flowing glacier. In Wilkes Land, Mertz Glacier splits around a high-ground region to reach Astrolabe trench to the west and Wilkes subglacial basin to the east. But Ninnis Glacier extends straight, deep south into Wilkes subglacial basin. These two glaciers exhibit an acceleration in flow at a bedrock step (20). A similar initiation is visible on one western tributary of Recovery Ice Stream and the western tributary of Totten, but over the vast majority of Antarctica we find no area where fast flow initiates at a bedrock step; instead, we observe tributary flow extending slowly, diffusively, and gradually from the flanks of ice divides.

Tributary shear margins, detected as zones of effective strain rate orders of magnitude higher than the background (Fig. 2A), appear at velocities of about 30 m/year, that is, at substantially smaller values than the 100 m/year quoted from the partial mapping of Siple Coast (14). This extensive network of shear margins reaches a few hundred km inland and expresses a strong coupling between coastal and inland flow of ice. Yet patterned enhanced flow initiates at even lower speed, in both West and East Antarctica. Patterned enhanced flow here means flow that is not uniform, dominated by deformational velocity, but includes a major basal-slip component that varies spatially as discussed next. Basal slip may be attributed to the presence of subglacial valleys that channelize thicker ice that generates more friction, more heat, and more melt water for lubrication and may also accumulate wet sediments that facilitate sliding or the presence of deformable or erodible, well-lubricated beds not tied in with bed topography (21). Bed conditions are poorly constrained by observations in Antarctica at present.

In Fig. 2D, we calculate the ice sheet deformational velocity by selecting an effective creep parameter A that best fits the data in a 200-km-wide band around the ice divides in Queen Maud Land, where internal deformation is expected to dominate ice motion [see Materials and Methods, supporting online material (SOM)]. Our calculation reproduces the ice motion pattern reasonably well over a larger domain, which provides confidence that this simple approach captures the general pattern of deformational velocity. Deformational and measured surface velocity start to differ within a few hundred km of ice divides, typically at velocities above about 15 m/year (fig. S3). The difference expresses uncertainties in A and ice thickness but for the most part

indicates the presence of basal slip, because the pattern of enhanced flow is quite different from the pattern of large deformational velocity. A doubling of *A* does not improve the model fit (fig. S4). In a second simulation, we calculate the deformational velocity obtained for a rigid bed (*21*), that is, where the speed only depends on the power of the driving stress, but the agreement between measured and deformational velocity is not improved (fig. S5). We conclude that basal slip is a significant component of ice motion in Antarctica, which develops at the flanks of ice divides.

This organization of ice sheet flow into a complex set of meandering, size-varying, speed-varying, anastomosing tributaries most certainly dominated by basal-slip motion challenges the view of ice sheet flow constrained by internal deformation and disconnected from the coastal regions, that was adopted as the background model for continental-scale ice sheet modeling (*6*, *21*). Actual observations of continental-scale ice motion reveal a new flow regime that initiates near topographic divides and involves a substantial amount of basal-slip motion. Much remains to be understood about the mechanisms of basal motion and patterned enhanced flow, but our observations already imply a tighter connection between coastal sectors and interior regions than in the hypothetical case of a uniform ice sheet flow, because the concentration of ice fluxes along preferred channels enhances the diffusivity of perturbations. It is likely that this patterned enhanced flow is not unique to Antarctica but is

a common feature of ice sheets. The mapping of Antarctic ice motion therefore redefines our view of ice sheet flow dynamics and the way ice sheets have been modeled in the past, with implications for improving reconstructions of past and ongoing changes and especially for modeling the evolution of ice sheet dynamics in a warming climate.

References and Notes

1. R. M. Goldstein, H. Engelhardt, B. Kamb, R. M. Frolich, *Science* **262**, 1525 (1993).
2. E. Rignot *et al.*, *Nat. Geosci.* **1**, 106 (2008).
3. J. L. Bamber, D. G. Vaughan, I. Joughin, *Science* **287**, 1248 (2000).
4. A. M. Le Brocq, A. J. Payne, M. J. Siegert, *Comput. Geosci.* **32**, 1780 (2006).
5. J. L. Bamber, E. Rignot, *J. Glaciol.* **48**, 237 (2002).
6. P. Lemke *et al.*, in *Climate Change 2007: The Physical Science Basis. Contribution of Working Group I to the Fourth Assessment Report of the Intergovernmental Panel on Climate Change*, S. Solomon *et al.*, Eds. (Cambridge Univ. Press, Cambridge, 2007).
7. K. C. Jezek, K. Farness, R. Carande, X. Wu, N. Labelle-Hammer, *Radio Sci.* **38**, 8067 (2003).
8. J. L. Bamber, J. Gomez-Dans, *Earth Planet. Sci. Lett.* **237**, 516 (2005).
9. E. Rignot *et al.*, *Geophys. Res. Lett.* **31**, L18401 (2004).
10. C. W. Swithinbank, in *Satellite Image Atlas of Glaciers of the World*, U.S. Geological Survey Professional Paper no. 1386-B (1988).
11. F. Pattyn, S. De Brabander, A. Huyghe, *Ann. Glaciol.* **40**, 225 (2005).
12. I. Allison, R. Frew, I. Knight, *Polar Rec.* **21**, 241 (1982).
13. A. Jenkins, S. S. Jacobs, *J. Geophys. Res.* **113**, C04013 (2008).
14. I. Joughin *et al.*, *Science* **286**, 283 (1999).
15. M. Stenoien, C. R. Bentley, *J. Geophys. Res.* **105**, 21761 (2000).
16. D. M. Rippin, J. L. Bamber, M. J. Siegert, D. G. Vaughan, H. F. J. Corr, *J. Geophys. Res.* **108**, 6008 (2003).
17. J. L. Bamber *et al.*, *Geology* **34**, 33 (2006).
18. R. E. Bell, M. Studinger, C. A. Shuman, M. A. Fahnestock, I. Joughin, *Nature* **445**, 904 (2007).
19. R. Kwok, M. J. Siegert, F. D. Carsey, *J. Glaciol.* **46**, 689 (2000).
20. N. F. Mc Intyre, *J. Glaciol.* **31**, 99 (1985).
21. K. Cuffey, W. S. B. Paterson, *The Physics of Glaciers* (Academic Press, Amsterdam, ed. 4, 2010).
22. T. Haran, J. Bohlander, T. Scambos, T. Painter, M. Fahnestock, MODIS (Moderate-Resolution Imaging Spectroradiometer) mosaic of Antarctica (MOA) image map (digital media) (National Snow and Ice Data Center, Boulder, CO, 2006).
23. E. Rignot, J. Mouginot, B. Scheuchl, *Geophys. Res. Lett.* **38**, L10504 (2011).
24. M. B. Lythe, D. G. Vaughan, *J. Geophys. Res.* **106**, 11335 (2001).

Aeroelastic Flutter Produces Hummingbird Feather Songs

Christopher J. Clark,[1] Damian O. Elias,[2] Richard O. Prum[1]

During courtship flights, males of some hummingbird species produce diverse sounds with tail feathers of varying shapes. We show that these sounds are produced by air flowing past a feather, causing it to aeroelastically flutter and generate flutter-induced sound. Scanning laser doppler vibrometry and high-speed video of individual feathers of different sizes and shapes in a wind tunnel revealed multiple vibratory modes that produce a range of acoustic frequencies and harmonic structures. Neighboring feathers can be aerodynamically coupled and flutter either at the same frequency, resulting in sympathetic vibrations that increase loudness, or at different frequencies, resulting in audible interaction frequencies. Aeroelastic flutter is intrinsic to stiff airfoils such as feathers and thus explains tonal sounds that are common in bird flight.

Feathers were a key innovation in the evolution of bird flight, providing a stiff, lightweight aerodynamic surface, or airfoil (*1*). As early designers of aircraft discovered, stiff, light airfoils in fast-flowing air are prone to aeroelastic flutter, whereby the airfoil oscillates at a frequency set by its stiffness and inertia, and aerodynamic forces (*2*). The acoustics of flutter is incompletely understood (*3*). However, in many birds, modified flight feathers are associated with the production of tonal flight sounds used in communication such as courtship displays (as in hummingbirds or snipe).

Hummingbirds are a clade of ~330 polygynous species in which males court females with showy ornaments, aerobatic displays, and vocal songs; females choose a mate from among available males (*4*). Independent of the humming of the wings for which hummingbirds are famous, males of the ~35 species in the "bee" hummingbird clade (*5*) produce tonal flight sounds, or courtship songs, during dive displays for females visiting their courtship territories. Although dive kinematics vary, a male generally ascends 5 to 40 m and then swoops down at high speed past the perched female, rapidly spreading and shutting his tail at the nadir of the dive and producing dive sounds in synchrony with each tail spread (*6–9*). In previous work, we have shown that tail feathers (or rectrices; R1, innermost, through R5, outermost) are both necessary and sufficient for the production of dive sounds: Experimental manipulation of specific tail feathers silences a male's dive sound, whereas these same feathers are sufficient to recreate the dive sound in lab experiments (*6–9*). We proposed that these dive sounds are produced by flutter (*6*) but did not measure flutter directly. In this work, we measured the vibrations of an array of hummingbird tail feathers in a wind tunnel directly, using a scanning laser doppler vibrometer (SLDV). We describe how aeroelastic flutter can result in a diverse array of audible sounds.

Air flowing past a feather provides aerodynamic energy that can cause flutter. We tested the relationship between air velocity (U_air) and feather

[1]Department of Ecology and Evolutionary Biology and Peabody Museum of Natural History, Post Office Box 208105, Yale University, New Haven, CT 06520, USA. [2]Environmental Science and Policy and Management, 137 Mulford Hall, University of California, Berkeley, Berkeley, CA 94720, USA.

Science

Ice Flow of the Antarctic Ice Sheet

E. Rignot, J. Mouginot and B. Scheuchl

ARTICLE TOOLS	http://science.sciencemag.org/content/333/6048/1427
SUPPLEMENTARY MATERIALS	http://science.sciencemag.org/content/suppl/2011/08/17/science.1208336.DC1
RELATED CONTENT	http://science.sciencemag.org/content/sci/333/6048/1357.6.full http://science.sciencemag.org/content/sci/333/6048/1386.full
REFERENCES	This article cites 27 articles, 4 of which you can access for free http://science.sciencemag.org/content/333/6048/1427#BIBL
PERMISSIONS	http://www.sciencemag.org/help/reprints-and-permissions